Electronic Supplementary Material (ESI) for Nanoscale.

Supporting Information

How Substituents Tune Quantum Interference in *meta*-OPE3 Molecular Junctions to Control Thermoelectric Transport

*Shen Yan [§a] , Yuxuan Luan [§a], Hailiang Xu [§bc], Hao Fan [§c], León Martin [§d], Arvind Kumar Gupta [c], Heiner Linke [*be], Edgar Meyhofer [*a], Pramod Reddy [*a], Fabian Pauly [*d], and Kenneth Wärnmark [*bc]*

[a] *Department of Mechanical Engineering, University of Michigan, Ann Arbor, MI 48109, USA*

[b] *NanoLund, Lund University, Box 118, 22100 Lund, Sweden*

[c] *Department of Chemistry, Centre of Analysis and Synthesis, Lund University, Box 121, 22100 Lund, Sweden*

[d] *Institute of Physics and Center for Advanced Analytics and Predictive Sciences, University of Augsburg, 86159 Augsburg, Germany*

[e] *Solid State Physics, Lund University, Box 118, 22100 Lund, Sweden*

Table of Contents

Part 1. General Information

Reactions were carried out at room temperature in the range of 20-23 °C. Anhydrous THF was distilled from sodium/benzophenone ketyl prior to use. Dry DCM was obtained from the solvent dispenser. All other solvents were ACS grade. The following reagents, 4-iodobenzenesulfonyl chloride, 2-chloro-2-methylpropane, ethynyltrimethylsilane (TMSA), dichloromethylsilane, 2,6-diiodo-4-nitroaniline, iodomethane, iron (Fe), acetyl chloride solution (AcCl, 1.0 M in DCM), potassium carbonate (K_2CO_3), sodium nitrite ($NaNO_2$), bis(triphenylphosphine)palladium(II) dichloride ($PdCl_2(PPh_3)_2$), triphenylphosphine (PPh_3), copper(I) iodide (CuI), *N,N*-diisopropylethylamine (DIPEA), titanium(IV) chloride solution ($TiCl_4$, 1.0 M in DCM) and triethylamine (Et_3N) were purchased, and used as received from Sigma Aldrich. The following compounds, 1-(*tert*-butylthio)-4-ethynylbenzene (**1**),[1-3] 2,4-diiodo-1-nitrobenzene (**2**),[4] 1,3-diiodo-5-nitrobenzene (**3**),[5] 2,4-diiodoaniline,[6] 3,5-diiodoaniline[7] and 3,5-diiodo-*N,N*-dimethylaniline (**5**)[8] were synthesized according to the literature. Column chromatography (ø x h, cm) was performed using silica gel (60 Å, 230-300 mesh, purchased from Sigma Aldrich) as solid support. All prepared compounds were transferred from the flasks into the small sample vessels using CH_2Cl_2 as the solvent. All NMR spectra were recorded on a Bruker Avance 400 MHz spectrometer. Deuterated solvents were used as received from Sigma Aldrich. ^{1}H NMR and ^{13}C NMR chemical shifts are reported in δ (ppm) units, parts per million (ppm) relative to the chemical shift of residual solvent; $CDCl_3$ (7.26 ppm for ^{1}H NMR spectra and 77.16 ppm for ^{13}C NMR spectra). The melting point was recorded on a micro melting point apparatus SMP3 (Stuart Scientific, UK) and corrected using standard compounds. IR spectra were recorded on a Bruker IR spectroment Alpha II. Electron spray ionization–high resolution mass (ESI–HRMS) spectra were recorded on a Waters Micromass Q-Tof micro mass spectrometer. Elemental analyses were performed by Mikroanalytisches Laboratorium KOLBE (Mülheim an der Ruhr, Germany).

Part 2. Details of Synthesis.

2,4-Diiodo-*N*,*N*-dimethylaniline (4). To a solution of 2,4-diiodoaniline (1.38 g, 4.00 mmol), K_2CO_3 (1.66 g, 12.0 mmol) in CH_3CN (20 mL), iodomethane (1.0 mL, 16 mmol) was added. The reaction mixture was stirred at reflux for 2 days. After cooling to rt, the reaction mixture was diluted with water (50 mL) and extracted with DCM (2 x 30 mL). The combined organic phases were dried over Na_2SO_4, filtrated, and evaporated to dryness *in vacuo*. The resulting residue was purified by silica gel chromatography (3 x 20, PE:EtOAc 97:3) to give compound **7** (1.35 g, 3.89 mmol) as a colorless liquid in 97% yield. R_f = 0.5 (PE:EtOAc 95:5). ^{1}H NMR (400 MHz, $CDCl_3$): δ (ppm) 8.13 (d, J = 2.0 Hz, 1H), 7.57 (dd, J = 8.4 and 2.0 Hz, 1H), 6.82 (d, J = 8.4 Hz, 1H), 2.74 (s, 6 H). ^{13}C NMR (100 MHz, $CDCl_3$): δ (ppm) 155.02, 147.7, 138.0, 122.3, 98.0, 87.1, 44.9. IR (neat): ν (cm^{-1}) 2940, 2827, 2780, 1476, 1463, 1450, 1158, 1017, 816. HRMS (ESI): m/z $[M+H]^+$ calc. for $C_8H_9NI_2$: 373.8903; Found: 373.8894. Anal. Calcd for $C_8H_9NI_2$: C 25.76, H 2.43, N 3.76. Found: C 25.88, H 2.67, N 3.70.

***General Procedure* 1 for the synthesis of acetylenes 6-9 using Sonogashira coupling 1-(tert-butylthio)-4-ethynylbenzene (1) substituted *meta*-diiodobenzenes (2-5).** To a pressure tube were added substituted *m*-diiodobenzenes **2-5** (1.0 equiv.), 1-(*tert*-butylthio)-4-ethynylbenzene (**1**) (2.2 equiv.), $PdCl_2(PPh_3)_2$ (0.05 equiv.), CuI (0.1 equiv.) and anhydrous Et_3N. The resulting mixture was degassed by bubbling nitrogen through the solution for 5 min. The tube was sealed and the reaction mixture was stirred at 40 °C for 12 h. After cooling to rt, the reaction mixture was diluted with water and extracted three times with DCM. The combined organic phases were dried over Na_2SO_4 , filtrated and evaporated to dryness *in vacuo*. The resulting residue was purified by silica gel chromatography (PE:EtOAc) to give **compounds 6-9**.

1,3-Bis((4-(*tert*-butylthio)phenyl)ethynyl)-4-nitrobenzene (6). This compound was prepared according to ***General Procedure 1***, using 1-(*tert*-butylthio)-4-ethynylbenzene (**1**) (0.21 g, 1.1 mmol), **2** (0.187 g, 0.500 mmol), $PdCl_2(PPh_3)_2$ (17.5 mg, 0.0250 mmol), CuI (9.5 mg, 0.050 mmol) and Et_3N (5 mL). After purification by silica gel chromatography (3 x 15, PE:EtOAc 96:4), compound **6** (0.238 g, 0.477 mmol) was isolated as a yellow solid in 95% yield. R_f = 0.5 (PE:EtOAc 92:8). Mp: 115-115.6 °C. ^{1}H NMR (400 MHz, $CDCl_3$): δ (ppm) 8.10 (d, J = 8.4 Hz, 1H), 7.86 (d, J = 1.6 Hz, 1H), 7.58-7.49 (m, 9H), 1.31 (s, 9H), 1.31 (s, 9H). ^{13}C NMR (100 MHz, $CDCl_3$): δ (ppm) 148.3, 137.5, 137.4, 137.3, 135.0, 132.4, 132.1, 131.8, 131.4, 128.8, 125.3, 122.6, 122.3, 119.2, 97.4, 94.2, 88.2, 85.8, 46.9, 46.8, 31.2. IR (neat): ν (cm^{-1}) 2960, 2922, 2212, 1599, 1519, 1335, 1165, 834. HRMS (ESI): m/z $[M+H]^+$ calc. for $C_{30}H_{29}NO_2S_2$: 500.1718; Found: 500.1709. Anal. Calcd for N 2.80; $C_{30}H_{29}NO_2S_2$•1/6 CH_2Cl_2: C 70.51, H 5.75, N 2.73. Found: C 70.68, H 5.78, N 2.73.

1,3-Bis((4-(*tert*-butylthio)phenyl)ethynyl)-5-nitrobenzene (7). This compound was prepared according to ***General Procedure 1***, using 1-(*tert*-butylthio)-4-ethynylbenzene (**1**) (0.21 g, 1.1 mmol), **3** (0.187 g, 0.500 mmol), $PdCl_2(PPh_3)_2$ (17.5 mg, 0.0250 mmol), CuI (9.5 mg, 0.050 mmol) and Et_3N (5 mL). After purification by silica gel chromatography (3 x 15, PE:EtOAc 97:3), compound **7** (0.235 g, 0.470 mmol) was isolated as a yellow solid in 94% yield. R_f = 0.6 (PE:EtOAc 95:5). Mp: 127-128.4 °C. ^{1}H NMR (400 MHz, $CDCl_3$): δ (ppm) 8.30 (d, J = 1.6 Hz, 2H), 7.96 (t, J = 1.6 Hz, 1H), 7.57-7.54 (m, 4H), 7.52-7.49 (m, 4H), 1.32 (s, 18H). ^{13}C NMR (100 MHz, $CDCl_3$): δ (ppm) 148.4, 139.8, 137.4, 134.8, 131.8, 125.9, 125.4, 122.4, 92.2, 87.8, 46.9, 31.2. IR (neat): ν (cm^{-1}) 2961, 2217, 1536, 1333, 1166, 833. HRMS (ESI): m/z $[M+H]^+$ calc. for $C_{30}H_{29}NO_2S_2$: 500.1718; Found: 500.1707. Anal. Calcd for $C_{30}H_{29}NO_2S_2$•3/10 H_2O: C 71.34, H 5.91, N 2.77. Found: C 71.32, H 5.86, N 2.76.

2,4-Bis((4-(*tert*-butylthio)phenyl)ethynyl)-*N*,*N*-dimethylaniline (8). This compound was prepared according to ***General Procedure 1***, using 1-(*tert*-butylthio)-4-ethynylbenzene (**1**) (0.209 g, 1.10 mmol), **4** (0.186 g, 0.499 mmol), $PdCl_2(PPh_3)_2$ (17.5 mg, 0.0249 mmol), CuI (9.5 mg, 0.050 mmol) and Et_3N (5 mL). After purification by silica gel chromatography (3 x 15, PE:EtOAc 97:3), compound **8** (0.236 g, 0.475 mmol) was isolated as a yellow oil in 95% yield. R_f = 0.5 (PE:EtOAc 95:5). ^{1}H NMR (400 MHz, $CDCl_3$): δ (ppm) 7.67 (d, J = 2.0 Hz, 1H), 7.53-7.44 (m, 8H), 7.39 (dd, J = 8.4 and 2.0 Hz, 1H), 6.87 (d, J = 8.4 Hz, 1H), 3.07 (s, 3H), 1.30 (s, 9H), 1.30 (s, 9H). ^{13}C NMR (100 MHz, $CDCl_3$): δ (ppm) 154.4, 154.4, 137.9, 137.4, 137.4, 133.3, 132.9, 132.8, 131.4, 131.2, 124.1, 116.7, 114.2, 113.8, 94.6, 90.7, 90.0, 88.1, 46.6, 46.5, 43.2, 31.1. IR (neat): ν (cm^{-1}) 2958, 2860, 2204, 1506, 1362, 1165, 1153, 831, 732. HRMS (ESI): m/z $[M+H]^+$ calc. for $C_{32}H_{35}NS_2$: 498.2289; Found: 498.2285. Anal. Calcd for $C_{32}H_{35}NS_2$•1/5 H_2O: C 76.66, H 7.12, N 2.79. Found: C 76.69, H 7.11, N 2.79.

3,5-Bis((4-(*tert*-butylthio)phenyl)ethynyl)-*N*,*N*-dimethylaniline (9). This compound was prepared according to ***General Procedure 1***, using 1-(*tert*-butylthio)-4-ethynylbenzene (**1**) (0.292 g, 1.53 mmol), **5** (0.26 g, 0.70 mmol), $PdCl_2(PPh_3)_2$ (24.6 mg, 0.0350 mmol), CuI (13.3 mg, 0.0698 mmol) and Et_3N (7 mL). After purification by silica gel chromatography (3 x 15, PE:EtOAc 97:3), compound **9** (0.302 g, 0.607 mmol) was isolated as a light yellow solid in 87% yield. R_f = 0.5 (PE:EtOAc 95:5). Mp: 137-138.1 ^{o}C. ^{1}H NMR (400 MHz, $CDCl_3$): δ (ppm) 7.53-7.47 (m, 8H), 7.08 (d, J = 1.2 Hz, 1H), 6.86 (s, 2H), 3.00 (s, 6H), 1.30 (s, 18H). ^{13}C NMR (100 MHz, $CDCl_3$): δ (ppm) 150.2, 137.4, 133.4, 131.7, 123.9, 123.7, 123.1, 115.7, 91.2, 88.4, 46.6, 40.6, 31.1. IR (neat): ν (cm^{-1}) 2959, 2895, 2210, 1582, 1483, 1166, 834. HRMS (ESI): m/z $[M+H]^+$ calc. for $C_{32}H_{35}NS_2$: 498.2289; Found: 498.2285. Anal. Calcd for $C_{32}H_{35}NS_2$•3/10 H_2O: C 76.39, H 7.13, N 2.78. Found: C 76.40, H 7.23, N 2.71.

General Procedure 2 for the Ti-mediated transformation of the *tert*-butyl thio-ethers 1b-4b into thio-acetates *meta*-OPE3 1-4. This method was adapted from the literature.[12] $TiCl_4$ (1.0 M in DCM, 3.0 equiv.) was added dropwise to a solution of compound **6-9** (1.0 equiv.) and acetyl chloride (1.0 M in DCM, 3.0 equiv.) in dry DCM at 0 °C. The resulting mixture was stirred under nitrogen atmosphere at rt for 4 h. The reaction mixture was diluted with H_2O and extracted with DCM. The combined organic phases were washed with brine, dried over Na_2SO_4, filtrated and evaporated to dryness *in vacuo*. The resulting residue was purified by silica gel chromatography (PE:EtOAc) to give compound ***meta*-OPE3 1-4**.

2,4-Bis((4-(acetylsulfanyl)phenyl)ethynyl)nitrobenzene (*meta*-OPE3 1). This compound was prepared according to ***General Procedure 2***, using **6** (0.225 g, 0.450 mmol), $TiCl_4$ (1.0 M in DCM, 1.35 mL, 1.35 mmol), acetyl chloride (1.0 M in DCM, 1.35 mL, 1.35 mmol) in dry DCM (11 mL). After purification by silica gel chromatography (3 x 15, PE:DCM 20:80), ***meta*-OPE3 1** (0.173 g, 0.367 mmol) was isolated as an orange solid in 82% yield. R_f = 0.5 (PE:DCM 20:80). Mp: 128.9 ^{o}C (dec.). ^{1}H NMR (400 MHz, $CDCl_3$): δ (ppm) 8.12 (d, J = 8.4 Hz, 1H), 7.87 (d, J = 1.6 Hz, 1H), 7.63 (dt, J = 8.4 and 2.0 Hz, 2H), 7.60-7.57 (m, 3H), 7.44 (dt, J = 8.0 and 1.6 Hz, 4H), 2.46 (s, 3H), 2.45 (s, 3H). ^{13}C NMR (100 MHz, $CDCl_3$): δ (ppm) 193.3, 193.2, 148.4, 137.6, 134.5, 134.4, 132.8, 132.5, 131.6, 129.7, 129.7, 128.7, 125.3, 123.5, 123.2, 119.1, 97.1, 93.9, 88.3, 85.9, 30.51, 30.50. IR (neat): ν (cm^{-1}) 2924, 2212, 1709, 1518, 1338, 1120, 829. HRMS (ESI): m/z $[M+Na]^+$ calc. for $C_{26}H_{17}NO_4S_2$: 494.0497; Found: 494.0488. Anal. Calcd for $C_{26}H_{17}NO_4S_2$•1/10 CH_2Cl_2: C 65.30, H 3.61, N 2.92, S 13.36. Found: C 65.53, H 3.73, N 2.86, S 13.07.

3,5-Bis((4-(acetylsulfanyl)phenyl)ethynyl)nitrobenzene (*meta*-OPE3 2). This compound was prepared according to ***General Procedure 2***, using **7** (0.30 g, 0.60 mmol), $TiCl_4$ (1.0 M in DCM, 1.80 mL, 1.80 mmol), acetyl chloride (1.0 M in DCM, 1.80 mL, 1.80 mmol) in DCM (15 mL).

After purification by silica gel chromatography (3 x 15, PE:DCM 40:60), ***meta*-OPE3 2** (0.230 g, 0.488 mmol) was isolated as a light yellow solid in 81% yield. R_f = 0.4 (PE:DCM 40:60). Mp: 175 °C (dec.). ^{1}H NMR (400 MHz, $CDCl_3$): δ (ppm) 8.31 (d, J = 1.2 Hz, 2H), 7.97 (t, J = 1.6 Hz, 1H), 7.58 (d, J = 8.0 Hz, 4H), 7.44 (d, J = 8.0 Hz, 4H), 2.45 (s, 6H). ^{13}C NMR (100 MHz, $CDCl_3$): δ (ppm) 193.3, 148.4, 139.9, 134.5, 132.5, 129.5, 126.0, 125.3, 123.2, 91.9, 87.8, 30.5. IR (neat): ν (cm^{-1}) 3082, 2923, 2219, 1709, 1536, 1356, 1119, 828. HRMS (ESI): m/z $[M+H]^+$ calc. for $C_{26}H_{17}NO_4S_2$: 472.0677; Found: 472.0684. Anal. Calcd for $C_{26}H_{17}NO_4S_2$•1/10 CH_2Cl_2: C 65.30, H 3.61, N 2.92, S 13.36. Found: C 65.21, H 3.69, N 2.90, S 13.31.

2,4-Bis((4-(acetylsulfanyl)phenyl)ethynyl)-*N*,*N*-dimethylaniline (*meta*-OPE3 3). This compound was prepared according to ***General Procedure 2***, using **8** (0.30 g, 0.60 mmol), $TiCl_4$ (1.0 M in DCM, 1.81 mL, 1.81 mmol), acetyl chloride (1.0 M in DCM, 1.81 mL, 1.81 mmol) in DCM (15 mL). After purification by silica gel chromatography (3 x 20, DCM) ***meta*-OPE3 3** (0.174 g, 0.371 mmol) was isolated as a deep yellow oil in 62% yield. R_f = 0.7 (DCM). ^{1}H NMR (400 MHz, $CDCl_3$): δ (ppm) 7.66 (d, J = 2.0 Hz, 1H), 7.54 (t, J = 8.4 Hz, 4H), 7.41-7.37 (m, 5H), 6.85 (d, J = 8.4 Hz, 1H), 3.07 (s, 6H), 2.44 (s, 3H), 2.43 (s, 3H). ^{13}C NMR (100 MHz, $CDCl_3$): δ (ppm) 193.7, 193.6, 154.6, 138.1, 134.4, 134.3, 132.9, 132.1, 131.9, 128.1, 127.7, 125.1, 125.0, 116.7, 114.0, 113.5, 94.3, 91.0, 90.3, 87.9, 43.2, 30.39, 30.37. IR (neat): ν(cm^{-1}) 2923, 2853, 2205, 1705, 1508, 1121, 1094, 949, 826. HRMS (ESI): m/z $[M+H]^+$ calc. for $C_{28}H_{23}NO_2S_2$: 470.1248; Found: 470.1242. Anal. Calcd for $C_{28}H_{23}NO_2S_2$: C 71.61, H 4.94, N 2.98, S 13.65. Found: C 71.74, H 5.07, N 2.99, S 13.49.

3,5-Bis((4-(acetylsulfanyl)phenyl)ethynyl)-*N*,*N*-dimethylaniline (*meta*-OPE3 4). This compound was prepared according to ***General Procedure 2***, using **9** (0.30 g, 0.60 mmol), $TiCl_4$ (1.0 M in DCM, 1.81 mL, 1.81 mmol), acetyl chloride (1.0 M in DCM, 1.81 mL, 1.81 mmol) in

DCM (15 mL). After purification by silica gel chromatography (3 x 15, PE:EtOAc 60:40) ***meta*-OPE3 4** (0.190 g, 0.405 mmol) was isolated as a light yellow solid in 67% yield. R_f = 0.4 (PE:EtOAc 40:60). Mp: 147 °C (dec.). ^{1}H NMR (400 MHz, $CDCl_3$): δ (ppm) 7.56 (d, J = 8.0 Hz, 4H), 7.40 (d, J = 8.0 Hz, 4H), 7.09 (s, 1H), 6.85 (d, J = 0.8 Hz, 2H), 3.00 (s, 6H), 2.44 (s, 6H). ^{13}C NMR (100 MHz, $CDCl_3$): δ (ppm) 193.6, 150.3, 134.4, 132.4, 128.2, 124.7, 123.7, 123.2, 115.7, 91.4, 88.2, 40.6, 30.4. IR (neat): ν (cm^{-1}) 2923, 2210, 1708, 1583, 1121, 828. HRMS (ESI): m/z $[M+H]^+$ calc. for $C_{28}H_{23}NO_2S_2$: 470.1248; Found: 470.1240. Anal. Calcd for $C_{28}H_{23}NO_2S_2$•1/5 H_2O: C 71.07, H 4.98, N 2.96, S 13.55. Found: C 71.05, H 5.00, N 2.94, S 13.51.

Part 3. NMR Spectra of New Compounds

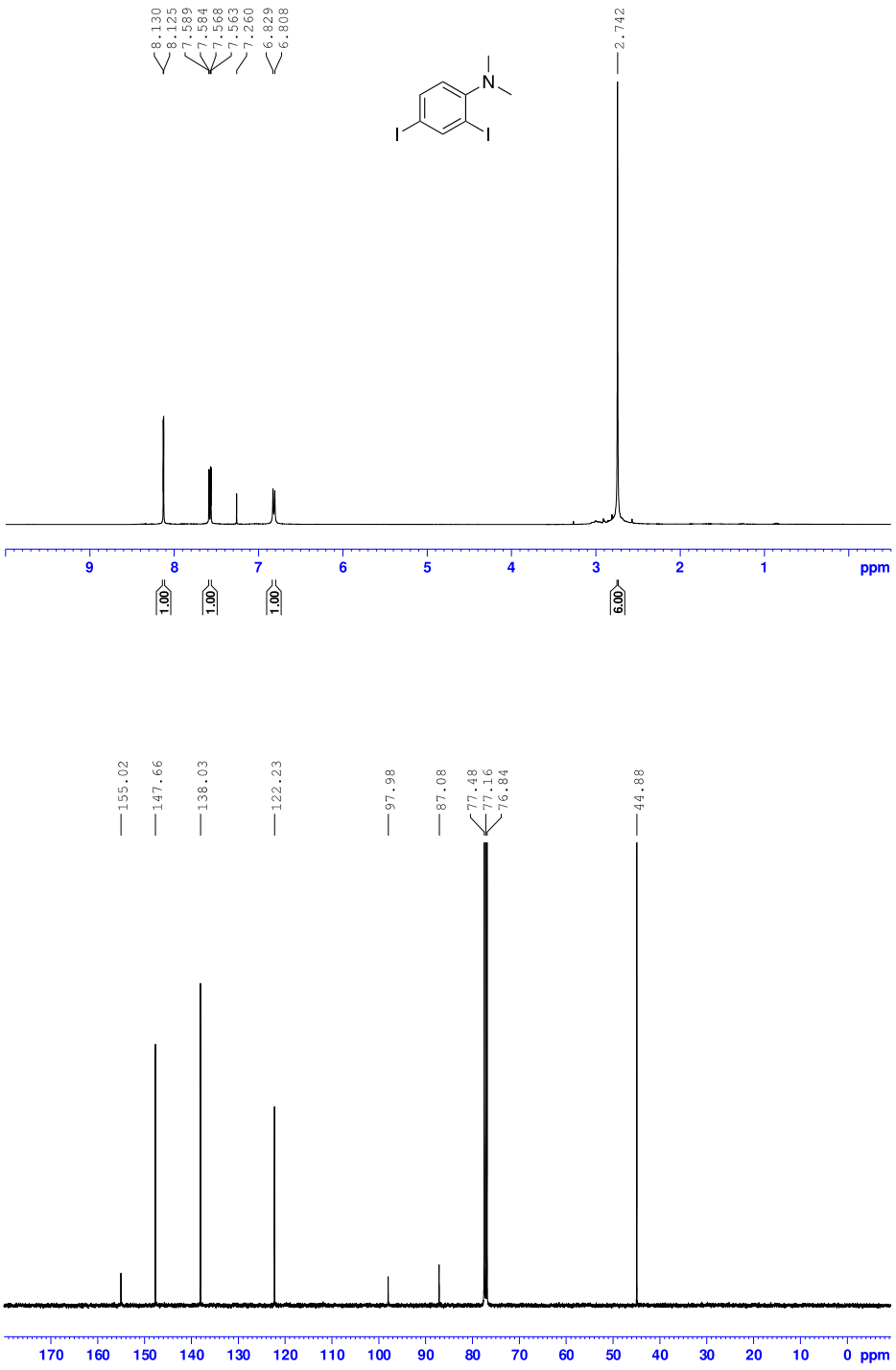

*Figure S1. ^{1}H (top) and ^{13}C (bottom) NMR spectra for compound **4** in $CDCl_3$.*

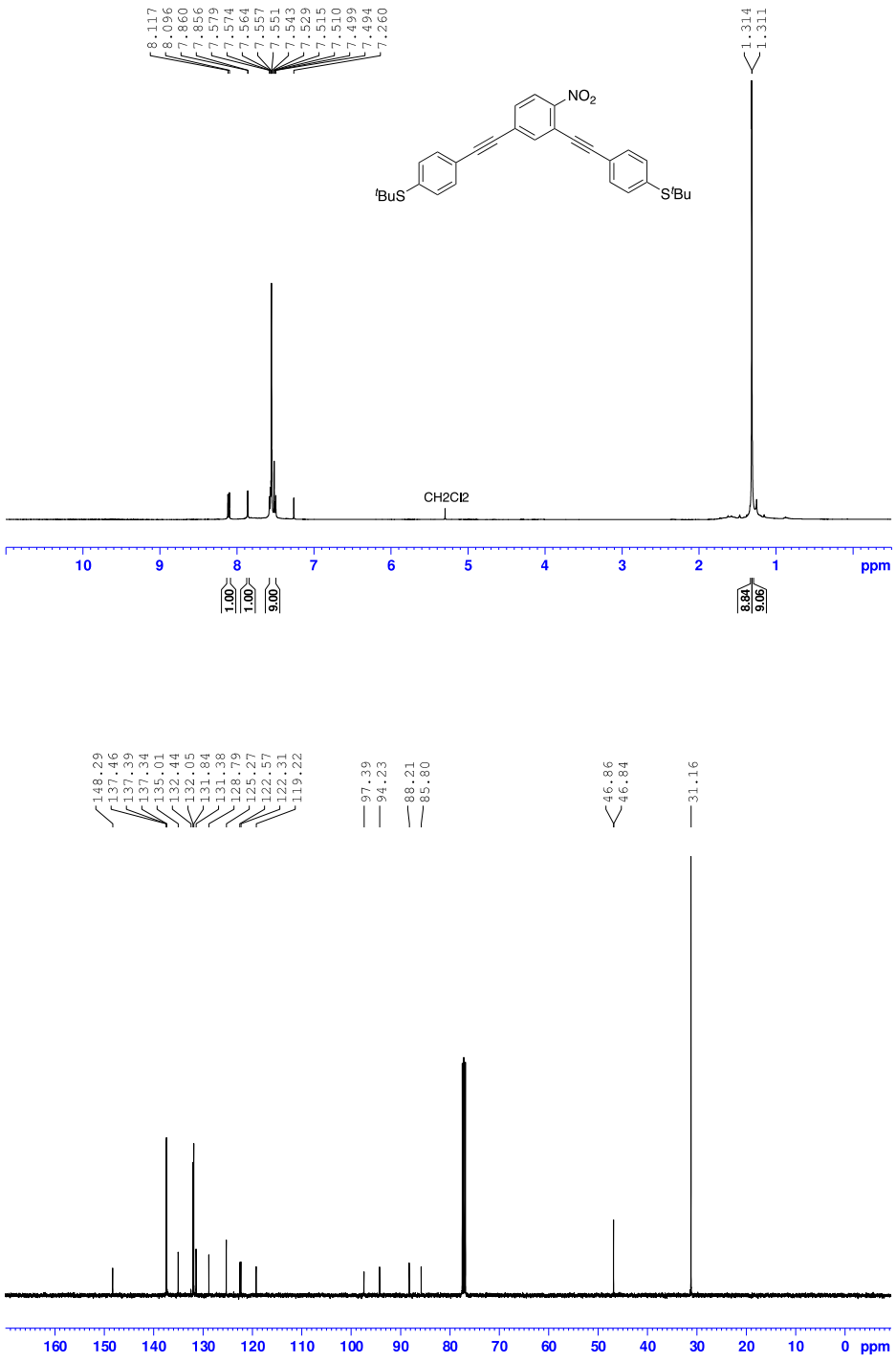

*Figure S2. ^{1}H (top) and ^{13}C (bottom) NMR spectra for compound **6** in $CDCl_3$.*

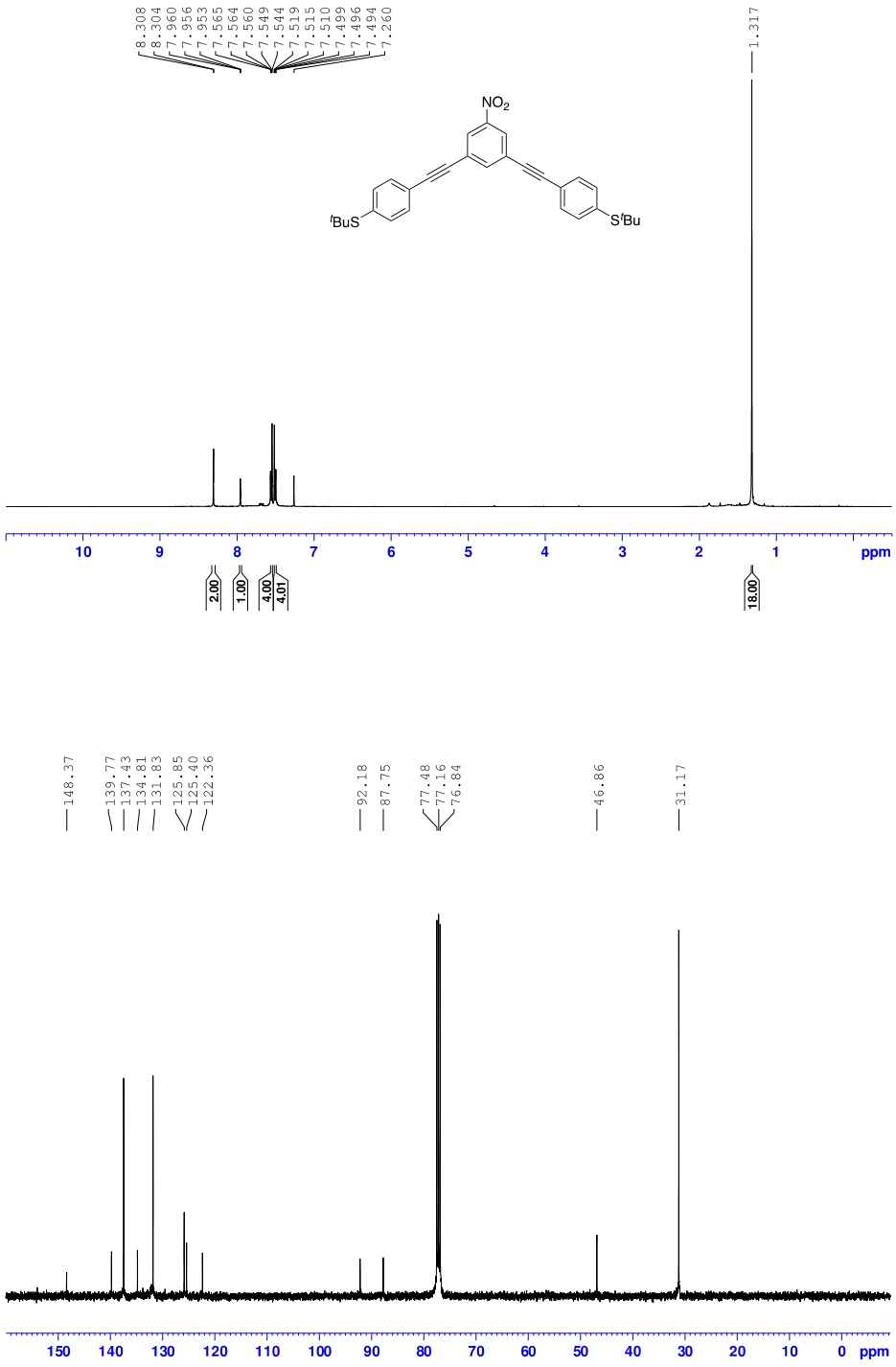

*Figure S3. ^{1}H (top) and ^{13}C (bottom) NMR spectra for compound **7** in $CDCl_3$.*

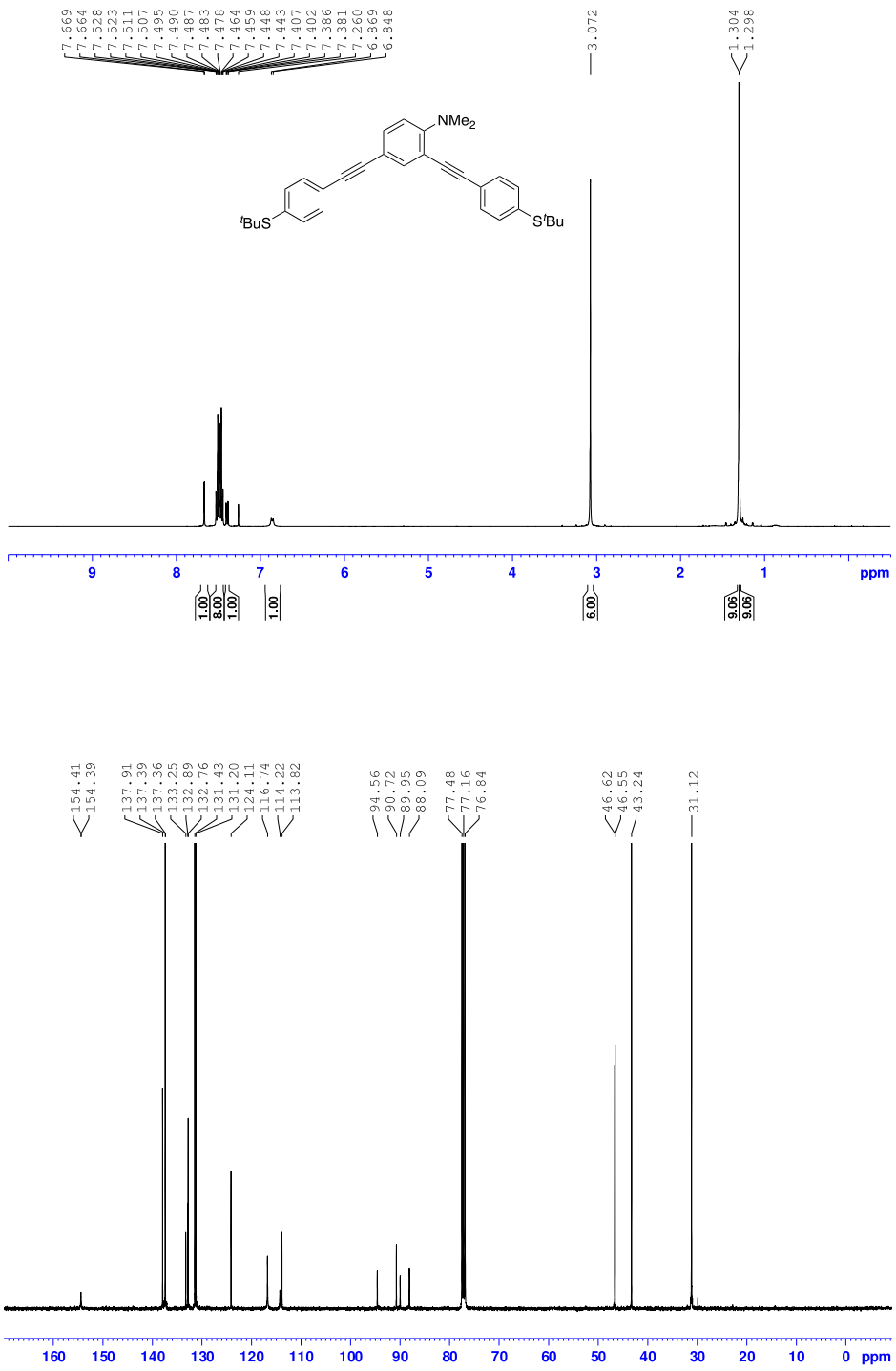

*Figure S4. ^{1}H (top) and ^{13}C (bottom) NMR spectra for compound **8** in $CDCl_3$.*

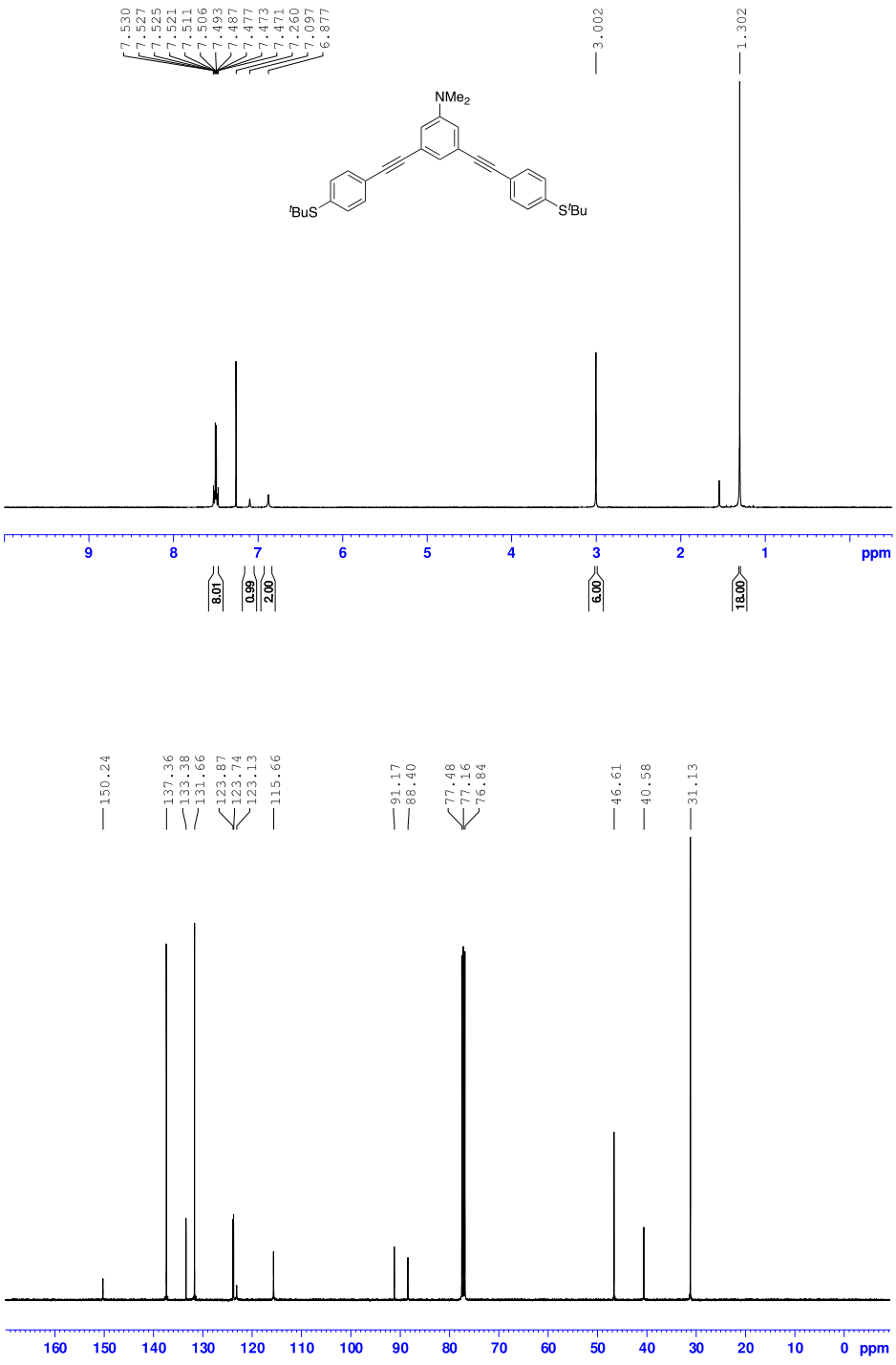

*Figure S5. ^{1}H (top) and ^{13}C (bottom) NMR spectra for compound **9** in $CDCl_3$.*

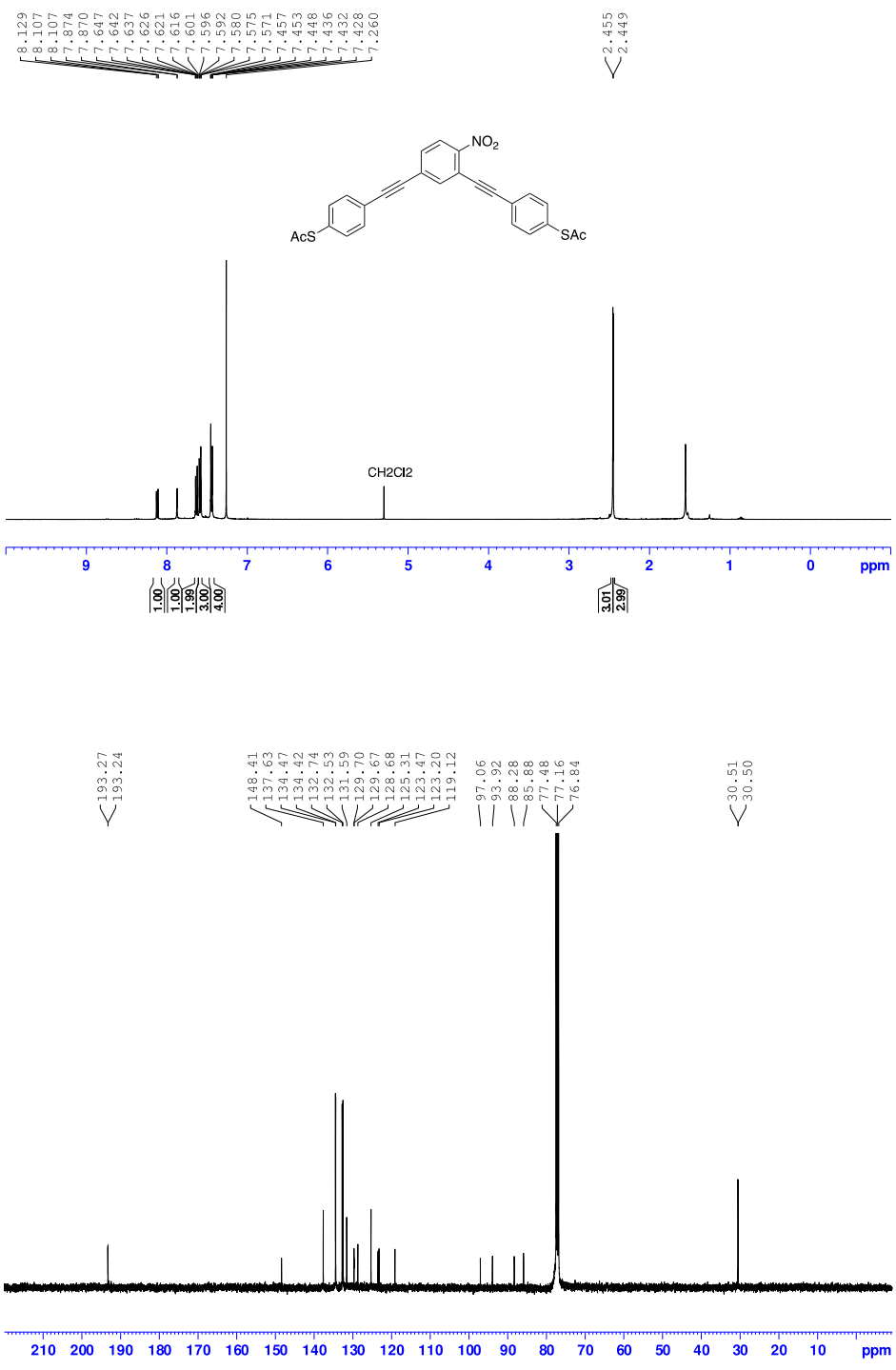

Figure S6. ^{1}H (top) and ^{13}C (bottom) NMR spectra for ***meta-OPE3 1*** *in* $CDCl_3$.

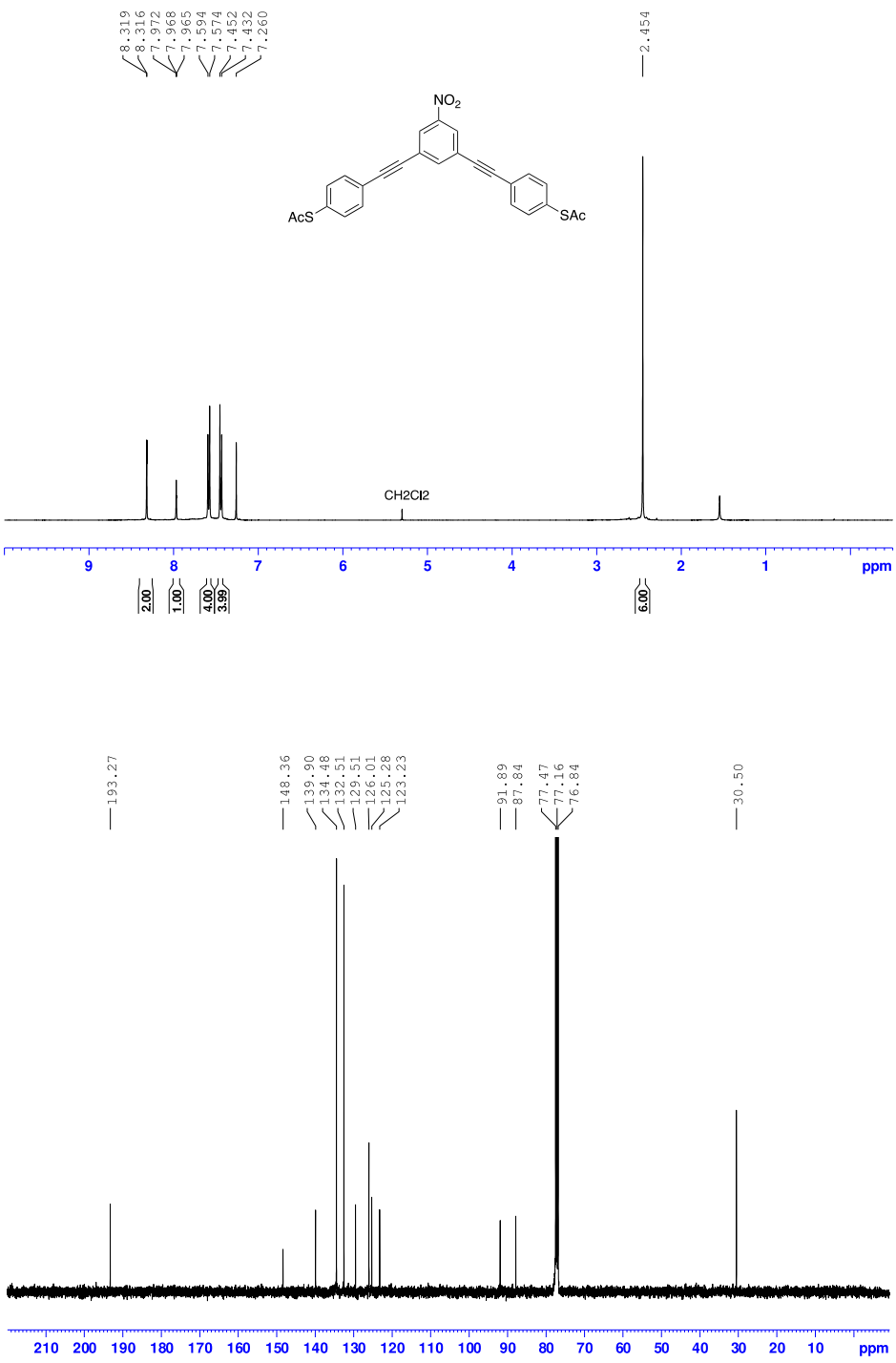

Figure S7. ^{1}H (top) and ^{13}C (bottom) NMR spectra for ***meta-OPE3 2*** *in* $CDCl_3$.

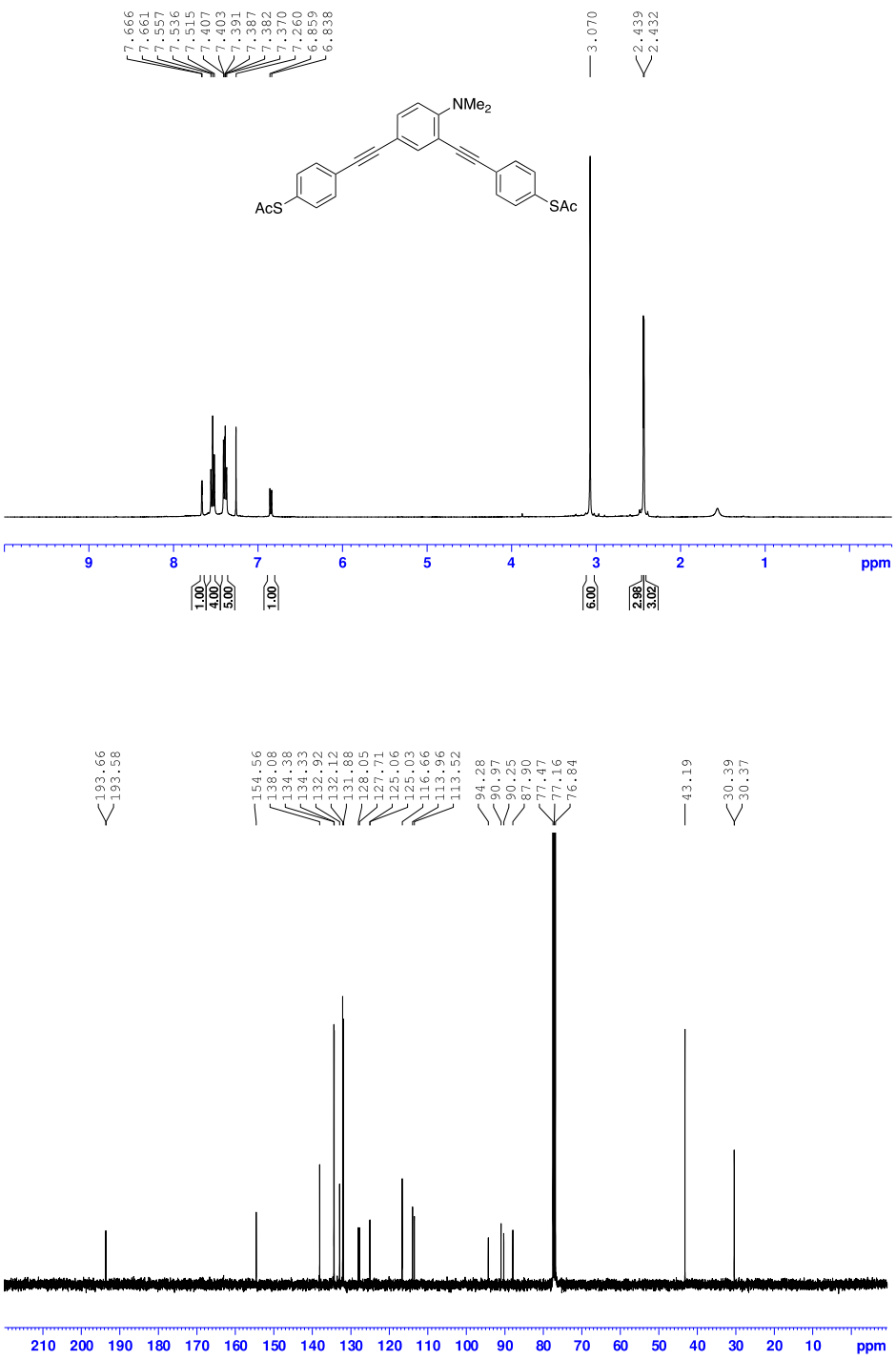

Figure S8. ^{1}H (top) and ^{13}C (bottom) NMR spectra for ***meta-OPE3 3*** *in* $CDCl_3$.

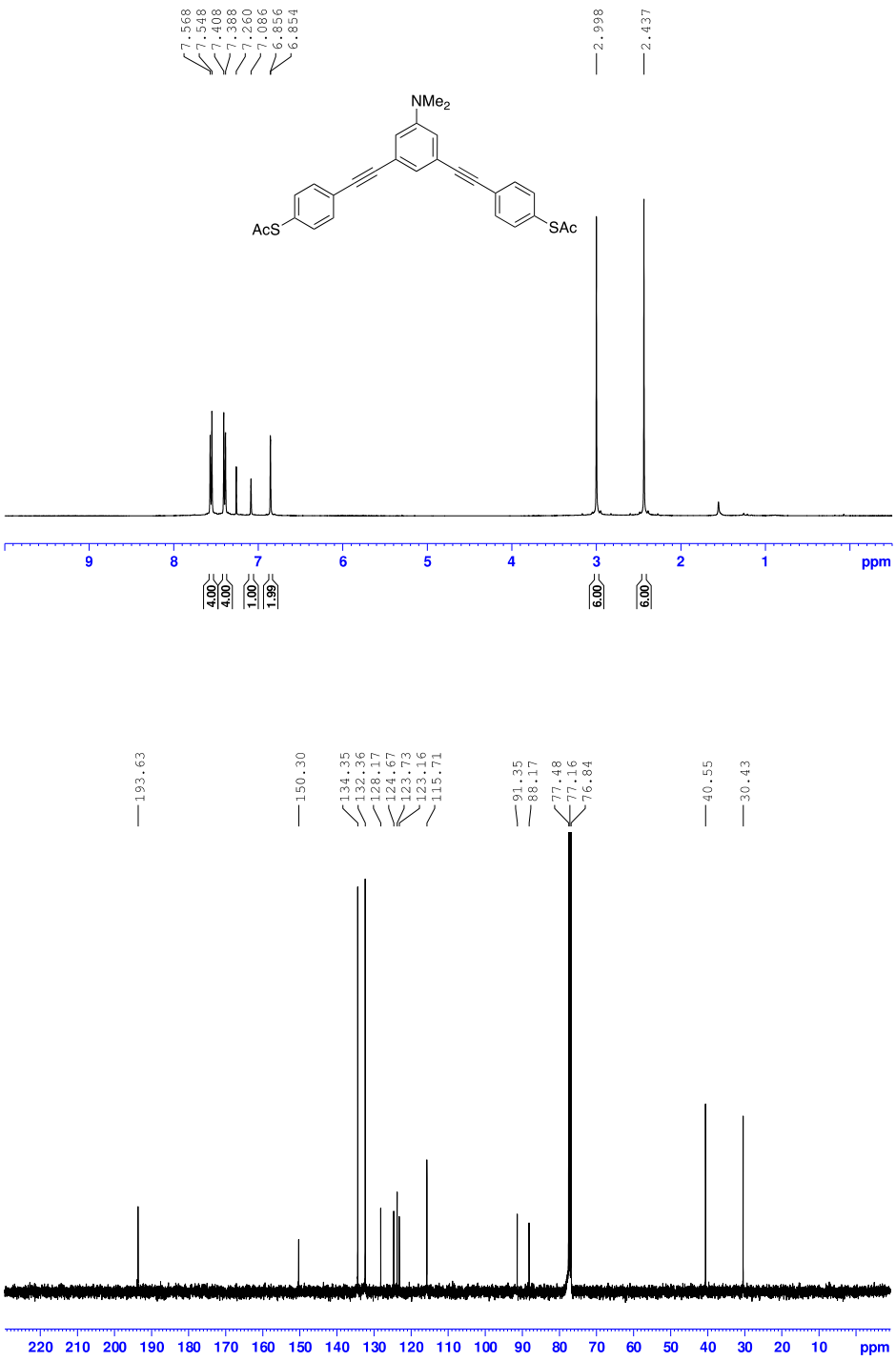

Figure S9. ^{1}H (top) and ^{13}C (bottom) NMR spectra for ***meta-OPE3 4*** *in* $CDCl_3$.

Part 4. Crystal X-ray Diffraction Analysis of *meta*-OPE3 1 and *meta*-OPE3 4

SC-XRD measurements were performed at 295 K using graphite-monochromatized Mo K_α radiation (λ = 0.71073 Å) on an Agilent Xcalibur Sapphire3 diffractometer high-brilliance IμS radiation source. The multi-scan empirical absorption correction with spherical harmonics was applied, as implemented in the SCALE3 ABSPACK scaling algorithm.[9] The structure was solved by direct methods and refined by full-matrix least-squares techniques against F2 using all data (SHELXT, SHELXS).[10, 11] All non-hydrogen atoms were refined with anisotropic displacement parameters if not stated otherwise. Hydrogen atoms were constrained in geometric positions to their parent atoms using the OLEX2 software.[12]

Table S1. Crystal data and structure refinement for ***meta-OPE3 1****.*

Identification code	***meta*-OPE3 1**	
Empirical formula	$C_{26}H_{17}NO_4S_2$	
CCDC No.	2300115	
Formula weight	471.52	
Temperature	295 K	
Wavelength	0.71073 Å	
Crystal system	Monoclinic	
Space group	P 1 21/c 1	
Unit cell dimensions	a = 11.7163(7) Å	a= 90°.
	b = 21.0713(9) Å	b= 116.822(8)°.
	c = 10.6802(6) Å	g = 90°.
Volume	2353.0(3) $Å^3$	
Z	4	
Density (calculated)	1.331 Mg/m^3	
Absorption coefficient	0.259 mm^{-1}	
F(000)	976	
Crystal size	0.28 x 0.2 x 0.12 mm^3	
Theta range for data collection	3.494 to 29.420°.	
Index ranges	-15<=h<=15, -29<=k<=28, -14<=l<=14	
Reflections collected	48471	
Independent reflections	5887 [R(int) = 0.0771]	
Completeness to theta = 25.242°	99.8 %	
Absorption correction	Semi-empirical from equivalents	
Max. and min. transmission	1.00000 and 0.89561	
Refinement method	Full-matrix least-squares on F^2	
Data / restraints / parameters	5887 / 12 / 300	
Goodness-of-fit on F^2	1.005	
Final R indices [I>2sigma(I)]	R1 = 0.0703, wR2 = 0.1802	
R indices (all data)	R1 = 0.2043, wR2 = 0.2354	
Extinction coefficient	n/a	
Largest diff. peak and hole	0.429 and -0.247 $e.Å^{-3}$	

*Table S2. Crystal data and structure refinement for **meta-OPE3 4**.*

Identification code	***meta*-OPE3 4**	
Empirical formula	$C_{28}H_{23}NO_2S_2$	
CCDC No.	2300114	
Formula weight	469.59	
Temperature	295 K	
Wavelength	0.71073 Å	
Crystal system	Triclinic	
Space group	P-1	
Unit cell dimensions	a = 8.6676(8) Å	a= 75.237(7)°.
	b = 10.3090(8) Å	b= 82.715(7)°.
	c = 15.1742(13) Å	g = 71.385(8)°.
Volume	1241.0(2) $Å^3$	
Z	2	
Density (calculated)	1.257 Mg/m^3	
Absorption coefficient	0.239 mm^{-1}	
F(000)	492	
Crystal size	0.36 x 0.22 x 0.16 mm^3	
Theta range for data collection	3.347 to 26.500°.	
Index ranges	-10<=h<=10, -12<=k<=12, -19<=l<=18	
Reflections collected	12068	
Independent reflections	5061 [R(int) = 0.0500]	
Completeness to theta = 25.242°	99.7 %	
Absorption correction	Semi-empirical from equivalents	
Max. and min. transmission	1.00000 and 0.96780	
Refinement method	Full-matrix least-squares on F^2	
Data / restraints / parameters	5061 / 0 / 302	
Goodness-of-fit on F^2	0.981	
Final R indices [I>2sigma(I)]	R1 = 0.0584, wR2 = 0.0976	
R indices (all data)	R1 = 0.1609, wR2 = 0.1383	
Extinction coefficient	n/a	
Largest diff. peak and hole	0.176 and -0.222 $e.Å^{-3}$	

*Table S3. Selected bond lengths and angles for **meta-OPE3 1** and **meta-OPE3 4.***

Compound	Bond lengths (Å)	Bond angles (°)
***meta*-OPE3 1**	C(2)-O(3): 1.181(5) C(2)-S(1): 1.763(6) C(12)-N(1): 1.461(5) C(22)-S(2): 1.765(4) C(25)-O(4): 1.188(4) C(25)-S(2): 1.774(4) N(1)-O(1): 1.178(5) N(1)-O(2): 1.157(5)	C(2)-O(3): 1.181(5) C(2)-S(1): 1.763(6) C(12)-N(1): 1.461(5) C(22)-S(2): 1.765(4) C(25)-O(4): 1.188(4) C(25)-S(2): 1.774(4) N(1)-O(1): 1.178(5) N(1)-O(2): 1.157(5) C(1)-C(2)-S(1): 111.2(4) O(3)-C(2)-C(1): 124.9(5)

		O(3)-C(2)-S(1): 123.9(4) C(4)-C(3)-S(1): 122.6(3) C(8)-C(3)-S(1): 118.2(3) C(11)-C(12)-N(1): 120.3(4) C(13)-C(12)-N(1): 117.5(4) C(21)-C(22)-S(2): 122.5(3) C(23)-C(22)-S(2): 119.1(3) C(26)-C(25)-S(2): 113.6(3) O(4)-C(25)-C(26): 123.5(4) O(4)-C(25)-S(2): 122.9(3) O(1)-N(1)-C(12): 120.3(5) O(2)-N(1)-C(12): 119.2(5) O(2)-N(1)-O(1): 120.5(5) C(3)-S(1)-C(2): 104.1(2) C(22)-S(2)-C(25): 102.57(17)
***meta*-OPE3 4**	C(1)-O(1): 1.196(4) C(1)-S(1): 1.777(5) C(3)-S(1): 1.761(3) C(13)-N(1): 1.372(4) C(17)-N(1): 1.447(4) C(18)-N(1): 1.440(3) C(24)-S(2): 1.770(3) C(27)-O(2): 1.196(3) C(27)-S(2): 1.788(4)	C(2)-C(1)-S(1): 111.1(3) O(1)-C(1)-C(2): 125.3(4) O(1)-C(1)-S(1): 123.6(3) C(4)-C(3)-S(1): 120.7(3) C(8)-C(3)-S(1): 120.1(3) N(1)-C(13)-C(12): 121.3(3) N(1)-C(13)-C(14): 121.3(3) O(2)-C(27)-S(2): 122.8(3) C(13)-N(1)-C(17): 120.8(3) C(13)-N(1)-C(18): 121.3(3) C(18)-N(1)-C(17): 117.9(3) C(3)-S(1)-C(1): 102.52(19) C(24)-S(2)-C(27): 100.49(16)

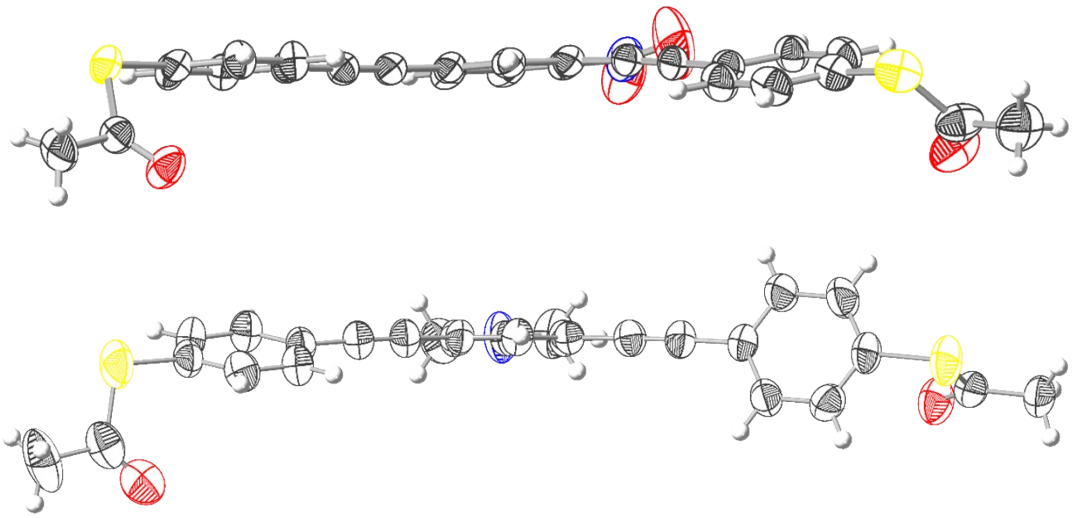

Figure S10. Side views of ***meta-OPE3 1*** *(top) and* ***meta-OPE3 4*** *(bottom).*

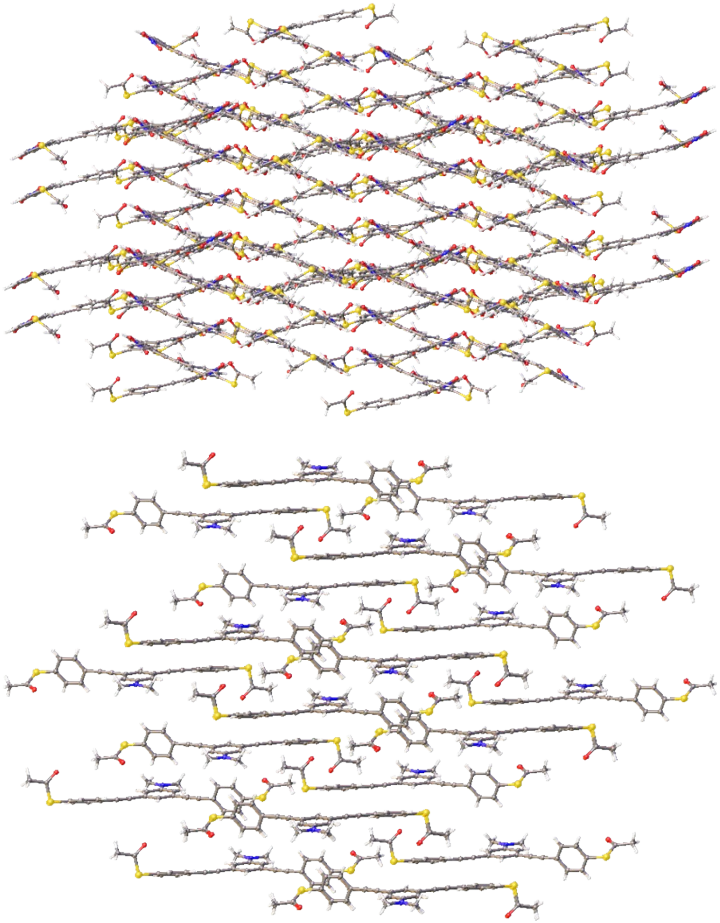

Figure S11. Packing diagrams of ***meta-OPE3 1*** *(top) and* ***meta-OPE3 4*** *(bottom).*

Part 5. Experimental Techniques

Sample preparation

Gold (Au) STM tips and template stripped samples with pristine Au films were prepared using an approach described in our past work.[13] Briefly, to form a molecular layer on the Au substrate, a 0.5 mM solution of the respective test molecules in dichloromethane solvent was drop-casted onto the freshly prepared Au template stripped sample for 3 hours to allow the adsorption of molecules. Subsequently, the prepared Au film, covered with a layer of test molecules, was carefully rinsed with ethanol and dried with high-purity nitrogen gas. The sample was immediately used for single molecule conductance and thermoelectricity measurements.

Electrical conductance measurements

The electrical conductance of single-molecule junctions was investigated using the scanning tunneling microscopy break-junction (STM-BJ) technique. All the measurements were conducted under ambient conditions (~50% relative humidity) at room temperature. In the STM-BJ measurements, a 100 mV constant DC voltage bias (V_{DC}) was applied between a Au STM tip and a freshly prepared template stripped Au sample on which a molecular layer was formed. First, the STM Au tip moved downwards to make contact with the Au substrate. Once an Au-Au contact was detected by the recorded electrical current flowing from the tip to the substrate, the Au tip was then retracted from the Au substrate at a constant speed of 0.2-0.4 nm/s, during which molecules were trapped stochastically between the tip and the substrate. The electrical current (I) was recorded during the tip retraction process with a low-noise current amplifier (DDPCA-300, FEMTO®) and later was converted to electrical conductance ($G = I/V_{DC}$). The formation of molecular junctions manifests itself through plateaus in the electrical conductance traces. The last

plateau before a junction ruptures, represents the single molecule junction. In order to determine the most probable single molecule conductance, we collected ~1000 traces to construct a linear-scale conductance histogram for each of the molecules and performed Gaussian fitting to the peaks of the obtained histograms. To demonstrate that our measured histogram data yield statistically robust most probable single molecule conductance peaks and that peak values are largely independent of the choice of model, we fitted the conductance data of ***meta*-OPE3 4**, shown in Fig. 3d, using both the Gaussian fit and the model used in Ref. 14 (see Eq. (3) in the reference). As visible in Fig. S12a, both peak shapes and peak values are consistent between the two different theoretical models, yielding $2.14\times10^{-6}\ G_0 \pm 0.01\times10^{-6}\ G_0$ for the Gaussian fit and $2.67\times10^{-6}\ G_0 \pm 0.27\times10^{-6}\ G_0$ for model in Ref. 14 (using the same conductance range from $10^{-6}G_0$ to $5\times10^{-6}G_0$ for both fits). Further, the goodness of fit (χ^2 p-value) is less than 0.05 (i.e., the confidence level of the fit is greater than 95%) in both models, which provides additional evidence that the obtained peak is statistically significant. To contrast these findings, we show in Fig. S12b data obtained in an experiment without molecules. The data is very different from that presented in Figs. 3 and S12a, confirming that the obtained peak shapes are indeed due to the formation of molecular junctions.

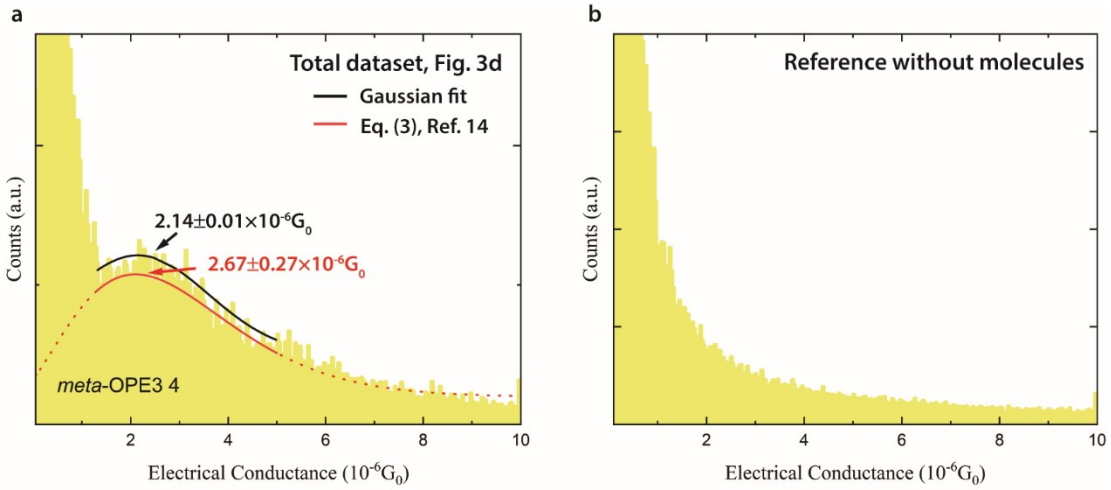

Fig. S12. (a) Fit to the experimental data shown in Fig. 3d of the manuscript using both the fit with a Gaussian function (Gaussian fit) and with the model proposed in Ref. 14 (see Eq. (3) in this reference). Obtained peak shapes and peak values (see the fits and numbers presented in the plot) are consistent. (b) The conductance histogram obtained in the absence of molecules is featureless without any statistically significant peaks.

In order to illustrate that ~1000 to 1500 conductance-distance traces are sufficient to accurately determine the electrical conductance of a single molecule junction, we evenly divided our dataset into three approximately equal parts (each contains ~300 to 500 traces) preserving the chronological order of the recording. We show the conductance histograms and fits of the peak in Fig. S13 (***meta*-OPE3 1,** for a peak at higher electrical conductance ~$10^{-5}G_0$) and Fig. S14 (***meta*-OPE3 2,** for a peak at lower electrical conductance ~$10^{-6}G_0$). Similar peak values and peak shapes are consistently observed for each of the subsets. Thus, even smaller datasets (with ~300 to 500 traces) lead to a reproducible peak at a virtually identical location with a similar width. This analysis confirms that our histograms, built from ~1000 consecutive traces, are sufficient to accurately determine the electrical conductance of single molecule junctions.

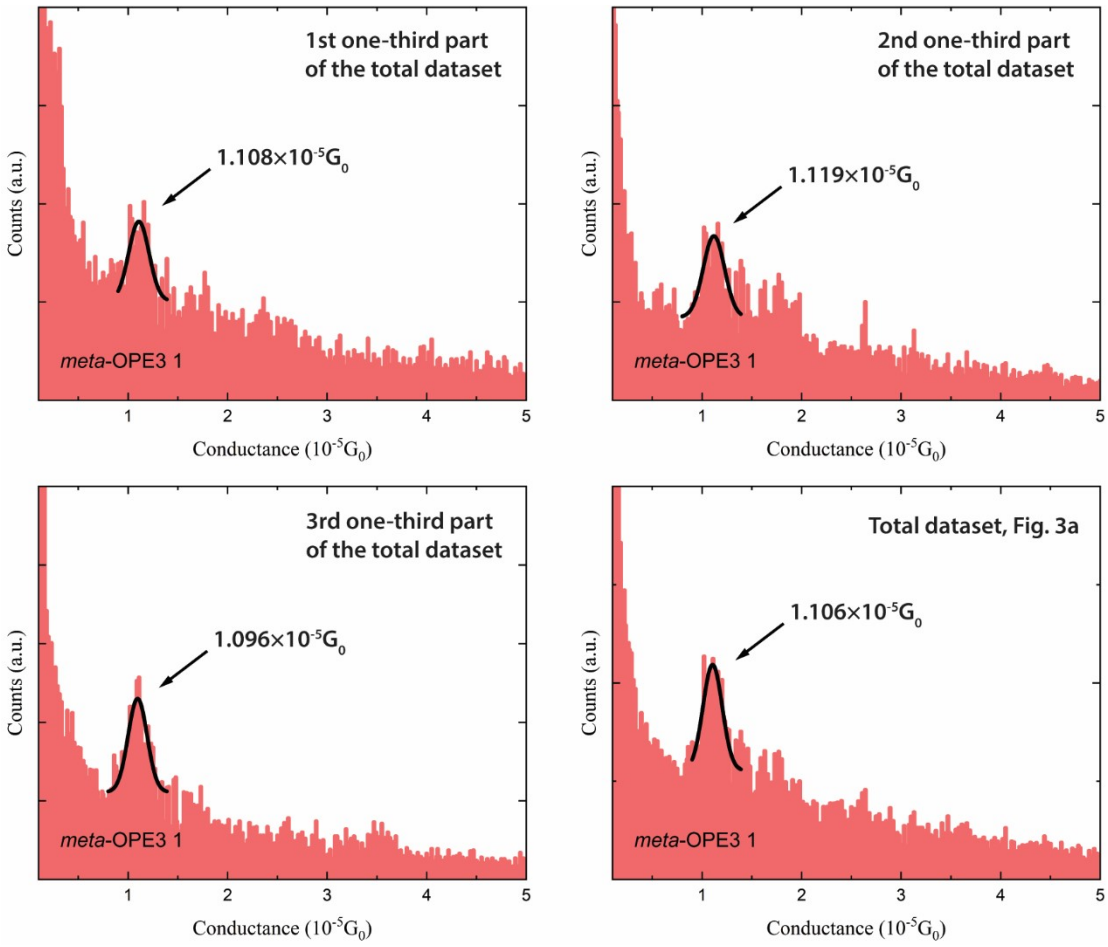

Fig. S13. Comparison of histograms of electrical conductance plotted using one-third of the total dataset and the full data for ***meta-OPE3 1****. The standard deviation of the four fitted peak values is ~10^{-7} G_0, which corresponds to less than 1% of the peak value.*

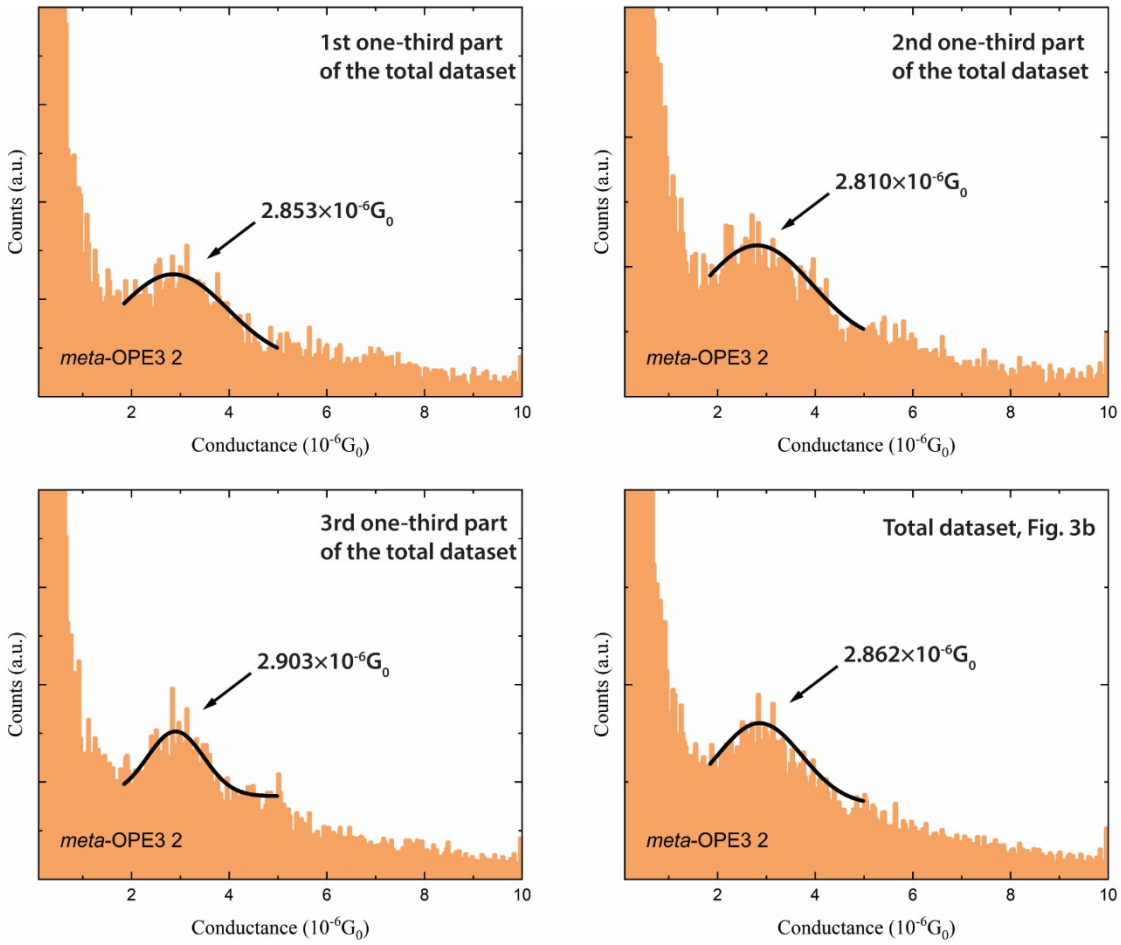

Fig. S14. Comparison of histograms of electrical conductance plotted using one-third of the total dataset and the full data for ***meta-OPE3 2****. The standard deviation of the four fitted peak values is ~4×10^{-8}G$_0$, which corresponds to less than 1.5% of the peak value.*

Seebeck coefficient measurements

Seebeck coefficient measurements of single molecule junctions were implemented by a modified STM-BJ method which is described in our past work.[13] To measure the thermoelectric properties of a molecular junction, the tip motion was modified from the approach described above for conductance measurements. Specifically, the tip withdrawal was stopped immediately once an electrical conductance value that is ±50% of the most probable conductance value in the linear-scale histogram (determined from the electrical conductance measurements described above) was reached. While the molecule was held between the tip and the substrate, the bias applied to the tip

was repeatedly switched between 100 mV and 0 mV with a duty cycle of 0.4 s until the junction ruptured. The currents flowing through the junctions under applied biases of 100 mV and 0 mV (with the substrate grounded and the bias applied to the tip) were recorded and used to determine the electrical conductance and Seebeck coefficient of the junction, respectively.

The short circuit thermoelectric current (I_{th}) flowing through the molecular junction, i.e., the electrical current induced by the applied temperature differential ($\Delta T = T_{substrate} - T_{tip}$) under zero applied voltage bias, and the electrical conductance (G) measured in the same switching cycle were used to estimate the expected open circuit thermoelectric voltage ($\Delta V_{TE} = V_{substrate} - V_{tip}$). where we define I_{th} to be positive when the short circuit thermoelectric current flows through the junction from the tip to the substrate. Based on this definition, we relate the expected open circuit thermoelectric voltage (ΔV_{TE}) to the measured short circuit thermoelectric current (I_{th}) and the electrical conductance (G) via: $\Delta V_{TE} = I_{th}/G$. The corresponding histograms of the thermoelectric voltage were first constructed using data obtained from over 5000 switching cycles (see Fig. 4 of the manuscript for a histogram), and the peak value of the histogram was estimated by fitting a Gaussian distribution to the histogram and identifying the maximum of the Gaussian distribution curve. Next, to obtain the Seebeck coefficient of the molecular junction we applied a linear fit to the measured values of ΔV_{TE}, obtained from the peaks of histograms corresponding to various temperature differentials (ΔT), and determined the Seebeck coefficient of the molecular junction ($S_{junction}$) using:

$$S_{junction} = -\frac{\Delta V_{TE}}{\Delta T} + S_{Cu} = -\frac{I_{th}}{G\Delta T} + S_{Cu}$$

Here, we include the Seebeck coefficient of copper (1.94 μV/K at T = 300 K) in the above equation, because a copper wire is involved in our measurements.

Part 6. Computational Details

Calculations for Isolated Molecules

Before discussing molecular junctions, we study the electronic structure of the isolated molecules, where the sulfur atoms are terminated by acetyl groups. All computations were carried out with the quantum chemistry program suite TURBOMOLE.[15] For density functional theory (DFT) calculations we used the exchange-correlation functional PBE.[16] As convergence criterion we employed "scfconv 8" for the total energy in DFT, geometry relaxations were performed within "gcart 3", and as basis set we chose "def-TZVP".[17]

Of special interest are the energies of the highest occupied molecular orbital (HOMO) and of the lowest unoccupied molecular orbital (LUMO) as well as the resulting energy gap. In Table S4, the corresponding values are shown for DFT.

Since DFT typically underestimates the energy gaps, we also use the ΔSCF method,[18] which is based on total energy differences between the neutral (N electrons) and charged molecules ($N \pm 1$ electrons). The electron affinity (EA)

$$EA = E_N^0 - E_{N+1}^0$$

and the ionization potential (IP)

$$IP = E_{N-1}^0 - E_N^0$$

are equivalent to the negative of the HOMO and LUMO energies and are shown together with the corresponding energy gap in Table S5.

Additionally, we use many-body perturbation theory (MBPT) in the *GW* approximation,[19-21] more precisely the linearized G_0W_0 and the eigenvalue self-consistent (ev*GW*) methods, where

the exchange-correlation potential of DFT is replaced by the *GW* self-energy. In G_0W_0 this self-energy is calculated once using the eigenenergies and eigenstates from the previous DFT calculation, leading to a first order correction of the DFT eigenvalues. The ev*GW* method employs the resulting eigenvalues to calculate a new *GW* self-energy and repeats the procedure until convergence is reached. In both G_0W_0 and ev*GW* approaches, however, the original eigenstates of the DFT calculation remain unchanged. Since we are most interested in the energy gap, we calculate HOMO and LUMO energies directly and shift all other molecular orbital energies in occupied and unoccupied sectors accordingly. The results are shown in Table S6 for the G_0W_0 method and in Table S7 for the ev*GW* method.

With all methods we observe that the HOMO-LUMO gaps are reduced for ***meta*-OPE3 1-4** compared to the original molecule ***meta*-OPE3**. This is due to additional electronic states inside the gap. Furthermore, we find a shift of both HOMO and LUMO to lower energies for the two molecules containing the electron-withdrawing nitro group, ***meta*-OPE3 1** and ***meta*-OPE3 2**, and a shift to higher energies for the two molecules containing the electron-donating dimetyl-amine group, ***meta*-OPE3 3** and ***meta*-OPE3 4**, reflecting the different electronic character of the two substituents.

Table S4. Calculated molecular energy levels and HOMO-LUMO gaps (eV) using DFT.

Molecule	HOMO	LUMO	HOMO-LUMO gap
***meta*-OPE3**	-5.39	-2.67	2.71
***meta*-OPE3 1**	-5.68	-3.61	2.08
***meta*-OPE3 2**	-5.71	-3.59	2.12
***meta*-OPE3 3**	-4.76	-2.50	2.25
***meta*-OPE3 4**	-4.85	-1.49	2.35

Table S5. Calculated molecular energy levels and HOMO-LUMO gaps (eV) using ΔSCF.

Molecule	HOMO	LUMO	gap
***meta*-OPE3**	-6.81	-1.28	5.53
***meta*-OPE3 1**	-7.09	-1.98	5.11
***meta*-OPE3 2**	-7.07	-1.74	5.33
***meta*-OPE3 3**	-6.30	-1.13	5.17
***meta*-OPE3 4**	-6.50	-1.54	5.35

Table S6. Calculated molecular energy levels and HOMO-LUMO gaps (eV) using G_0W_0.

Molecule	HOMO	LUMO	HOMO-LUMO gap
***meta*-OPE3**	-6.83	-0.66	6.17
***meta*-OPE3 1**	-7.08	-1.60	5.48
***meta*-OPE3 2**	-7.15	-1.16	5.99
***meta*-OPE3 3**	-6.09	-0.53	5.56
***meta*-OPE3 4**	-6.32	-0.50	5.82

Table S7. Calculated molecular energy levels and HOMO-LUMO gaps (eV) using evGW.

Molecule	HOMO	LUMO	HOMO-LUMO gap
***meta*-OPE3**	-7.25	-0.06	7.19
***meta*-OPE3 1**	-7.57	-0.96	6.61
***meta*-OPE3 2**	-7.63	-0.40	7.23
***meta*-OPE3 3**	-6.62	0.06	6.68
***meta*-OPE3 4**	-6.96	0.08	7.04

Construction of Molecular Junctions and Discussion of DFT Transmission Curves

As described in the main paper, we study two different junction geometries, the hollow-hollow (HH) and top-top (TT) configurations. In the TT case, the extended central cluster (ECC)[22] consists of the molecule and 20 gold atoms on each side, which is reduced to 19 per side in the HH case. The last two gold layers of each tip are treated as part of semiinfinite electrodes in the transport

calculations.[22] They are therefore kept fixed during the geometry optimization of the junction. The molecule and a total of 8 gold atoms in the TT geometries and 6 gold atoms in the HH geometries, respectively, are hence relaxed using the default criterion "gcart 3". All DFT calculations for junctions use the def-SV(P) basis set[23] and PBE[16] as exchange-correlation functional. They are converged in energy within "scfconv 8".

In Fig. S12a and S12b, we show the transmission curves based on DFT. If we compare the transmissions of the ***meta*-OPE3** derivatives with those of the parent ***meta*-OPE3**, we find additional peaks inside the original HOMO-LUMO gap. This is similar to the behavior discussed for the DFT+Σ scheme in the main paper (see Fig. 5). For ***meta*-OPE3 2** and ***meta*-OPE3 4** we find Fano-like antiresonances[24, 25] at energies of around -3.6 eV and -5.1 eV, respectively, while there are regular transmission maxima for ***meta*-OPE3 1** and ***meta*-OPE3 3** at energies of -3.8 eV and -5.0 eV, respectively. The energetic position of the features relates to the electronic character of the substituent, while the type of resonance is related to the attachment point. For a better understanding, we plot the orbitals responsible for these additional features in Fig. S12c. We observe that the molecular orbital is very localized in the center of the molecule for the symmetric attachment of the side group, as in ***meta*-OPE3 2** and ***meta*-OPE4**, which leads to the aforementioned Fano antiresonance. For the unsymmetric positioning, as it is the case in ***meta*-OPE3 1** and ***meta*-OPE3 3**, the molecular orbital is extended further over the backbone of the molecule and better coupled to the electrodes. It thus contributes to the electronic transport as a regular transmission resonance. The side groups in the symmetric attachment have less influence on the destructive quantum interference inside the HOMO-LUMO gap. For the unsymmetric attachment, in contrast, the transmission minimum is strongly shifted to lower or higher energies of around -5 eV or -3 eV for ***meta*-OPE3 1** and ***meta*-OPE3 3**, respectively.

These observations already lead to a qualitative understanding of the electronic transport properties. Using a Fermi energy of -5 eV, we find however quantitative discrepancies between computed and measured conductance and thermopower values, presented in Tables S8 and 1. To improve on these shortcomings, we applied the DFT+Σ correction scheme, as presented in the main text.

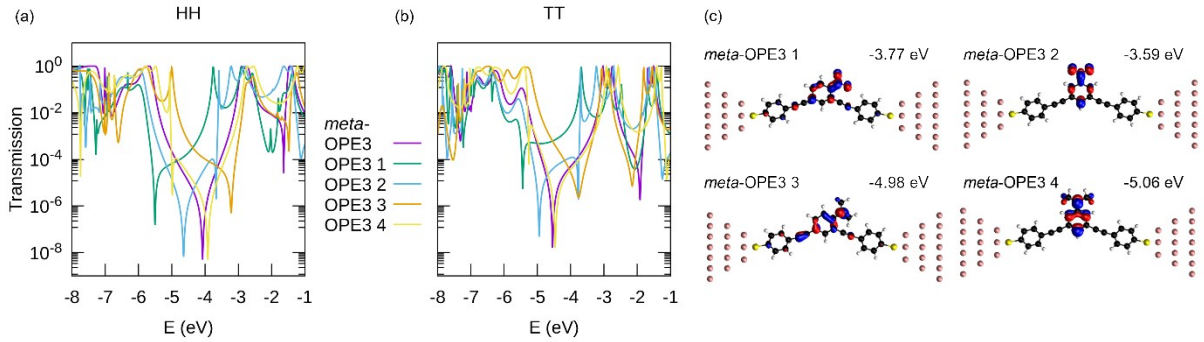

*Figure S12. (a) Transmission curves based on DFT calculations for the **meta-OPE3** molecule and its derivatives in the hollow-hollow (HH) junction geometries. (b) Same as (a) for top-top (TT) junction geometries. (c) Orbitals causing the additional peaks inside the HOMO-LUMO gap for **meta-OPE3 1-4** from top left to bottom right in the HH geometry. The energies of the orbitals are indicated. To allow for a consistent comparison, all plots of molecular orbitals use the same isovalues.*

*Table S8. Calculated single-molecule conductances and thermopowers of **meta-OPE3** and **meta-OPE3 1-4** based on the DFT approach for HH and TT junction geometries, using a Fermi energy of -5 eV.*

Molecule	G (G_0) [HH]	G (G_0) [TT]	S (μV/K) [HH]	S (μV/K) [TT]
***meta*-OPE3**	2.39×10^{-4}	4.68×10^{-4}	54.3	91.7
***meta*-OPE3 1**	6.51×10^{-5}	4.8×10^{-4}	-12.2	2.4
***meta*-OPE3 2**	1.56×10^{-5}	7.24×10^{-6}	63.5	218.4
***meta*-OPE3 3**	4.45×10^{-1}	2.92×10^{-2}	0.8	110.5
***meta*-OPE3 4**	2.44×10^{-2}	6.64×10^{-4}	198.5	80.0

Computational Details of DFT+Σ Calculations for Molecular Junctions

In the DFT+Σ approach all occupied levels of the molecular subspace are shifted down in energy by Σ_{occ}, whereas the virtual (or unoccupied) levels are shifted up by Σ_{vrt}, before the transmission function is calculated. The corresponding shifts are defined as

$$\Sigma_{vrt} = -\mathrm{EA} - \epsilon_{\mathrm{L}} - \Delta_{vrt} \ ,$$

$$\Sigma_{occ} = -\mathrm{IP} - \epsilon_{\mathrm{H}} + \Delta_{occ} \ .$$

Here EA and IP are the electron affinity and ionization potential, resulting from the ΔSCF calculation of the isolated molecule, see the discussion above. ϵ_L and ϵ_H are the DFT energies of the LUMO and HOMO of the isolated molecule, respectively. The shifts Δ_{occ} and Δ_{vrt} are so-called image charge corrections based on the potential energy of the charge distribution of the respective molecular orbital between two parallel metal plates. For the calculation of the image charges we follow the procedure described in Ref. 26 and place the metal planes 1.47 Å in front of the first unrelaxed gold layer. Different to the calculations for the isolated molecules, discussed above, we use the same def-SV(P)[23] basis set as in the junctions, and the geometry of the molecule is identical to those inside the junction apart from hydrogen atoms that we added to saturate the sulfur atoms.

References

1. K. Liu, X. Wang and F. Wang, *ACS Nano*, 2008, **2**, 2315-2323.
2. J. Ma, M. Vollmann, H. Menzel, S. Pohle and H. Butenschön, *J. Inorg. Organomet. Polym. Mater.*, 2008, **18**, 41-50.
3. T. Yamakawa, E. Ideue, Y. Iwaki, A. Sato, H. Tokuyama, J. Shimokawa and T. Fukuyama, *Tetrahedron*, 2011, **67**, 6547-6560.
4. Z. Zhang, Z. Zha, C. Gan, C. Pan, Y. Zhou, Z. Wang and M.-M. Zhou, *J. Org. Chem.*, 2006, **71**, 4339-4342.
5. S. H. Chanteau and J. M. Tour, *J. Org. Chem.*, 2003, **68**, 8750-8766.
6. R. Sakai, A. Nagai, Y. Tago, S.-i. Sato, Y. Nishimura, T. Arai, T. Satoh and T. Kakuchi, *Macromolecules*, 2012, **45**, 4122-4127.
7. Y. Feng, H. Chen, Z. X. Liu, Y. M. He and Q. H. Fan, *Chem. Eur. J.*, 2016, **22**, 4980-4990.
8. A. J. Martínez-Martínez, A. R. Kennedy, R. E. Mulvey and C. T. O'Hara, *Science*, 2014, **346**, 834-837.
9. *CrysAlis PRO, version 1.171.35.6*, Agilent Technologies, 2011.
10. G. M. Sheldrick, *Acta Crystallogr.*, 2008, **64**, 112-122.
11. G. M. Sheldrick, *Acta Crystallogr.*, 2015, **71**, 3-8.
12. O. V. Dolomanov, L. J. Bourhis, R. J. Gildea, J. A. Howard and H. Puschmann, *J. Appl. Crystallogr.*, 2009, **42**, 339-341.
13. H. Xu, H. Fan, Y. Luan, S. Yan, L. Martin, R. Miao, F. Pauly, E. Meyhofer, P. Reddy, H. Linke and K. Wärnmark, *J. Am. Chem. Soc.*, 2023, **145**, 23541-23555.
14. R. Frisenda, M. L. Perrin, H. Valkenier, J. C. Hummelen and H. S. J. van der Zant, *Physica Status Solidi (b)*, 2013, **250**, 2431-2436.
15. Y. J. Franzke, C. Holzer, J. H. Andersen, T. Begušić, F. Bruder, S. Coriani, F. D. Sala, E. Fabiano, D. A. Fedotov, S. Fürst, S. Gillhuber, R. Grotjahn, M. Kaupp, M. Kehry, M. Krstić, F. Mack, S. Majumdar, B. D. Nguyen, S. M. Parker, F. Pauly, A. Pausch, E. Perlt, G. S. Phun, A. Rajabi, D. Rappoport, B. Samal, T. Schrader, M. Sharma, E. Tapavicza, R. S. Treß, V. Voora, A. Wodyński, J. M. Yu, B. Zerulla, F. Furche, C. Hättig, M. Sierka, D. P. Tew and F. Weigend, *J. Chem. Theory Comput.*, 2023, **19**, 6859-6890.
16. J. P. Perdew, K. Burke and M. Ernzerhof, *Phys. Rev. Lett.*, 1996, **77**, 3865. Erratum *Phys. Rev. Lett.* 1997, **78**, 1396.
17. A. Schäfer, C. Huber and R. Ahlrichs, *J. Chem. Phys.*, 1994, **100**, 5829-5835.
18. R. M. Martin, *Electronic Structure: Basic Theory and Practical Methods*, Cambridge University Press, 2nd Edition, 2020.
19. F. Kaplan, M. E. Harding, C. Seiler, F. Weigend, F. Evers and M. J. van Setten, *J. Chem. Theory Comput.*, 2016, **12**, 2528-2541.
20. M. J. van Setten, F. Weigend and F. Evers, *J. Chem. Theory Comput.*, 2013, **9**, 232-246.
21. L. Hedin, *Phys. Rev.*, 1965, **139**, A796.
22. F. Pauly, J. K. Viljas, U. Huniar, M. Häfner, S. Wohlthat, M. Bürkle, J. C. Cuevas and G. Schön, *New J. Phys.*, 2008, **10**, 125019.
23. A. Schäfer, H. Horn and R. Ahlrichs, *J. Chem. Phys.*, 1992, **97**, 2571-2577.
24. U. Fano, *Phys. Rev.*, 1961, **124**, 1866.
25. J. C. Cuevas and E. Scheer, *Molecular Electronics: An Introduction to Theory and Experiment, 2nd Edition*, World Scientific, 2017.
26. L. A. Zotti, M. Bürkle, F. Pauly, W. Lee, K. Kim, W. Jeong, Y. Asai, P. Reddy and J. C. Cuevas, *New J. Phys.*, 2014, **16**, 015004.